PAPER

Tunneling dynamics of an oscillating universe model

Journal of Cosmology and Astroparticle Physics
An IOP and SISSA journal

Tunneling dynamics of an oscillating universe model

Martin Bojowald and Pip Petersen[1]

Department of Physics The Pennsylvania State University,
104 Davey Lab, University Park, PA 16802, U.S.A.

E-mail: bojowald@psu.edu, sxp1171@case.edu

Received October 19, 2021
Revised March 17, 2022
Accepted April 3, 2022
Published May 5, 2022

Abstract. Quasiclassical methods for non-adiabatic quantum dynamics can reveal new features of quantum effects, such as tunneling evolution, that are harder to analyze in standard treatments based on wave functions of stationary states. Here, these methods are applied to an oscillating universe model introduced recently. Our quasiclassical treatment correctly describes several expected features of tunneling states, in particular just before and after tunneling into a trapped region where a model universe may oscillate through many cycles of collapse and expansion. As a new result, the oscillating dynamics is found to be much less regular than in the classical description, revealing a succession of cycles with varying maximal volume even when the matter ingredients and their parameters do not change.

Keywords: quantum cosmology, cosmic singularity

ArXiv ePrint: 2110.09491

[1]New address: Department of Physics, Case Western Reserve University, 2076 Adelbert Road, Cleveland, OH 44106, U.S.A.

https://doi.org/10.1088/1475-7516/2022/05/007

JCAP05(2022)007

Contents

JCAP05(2022)007

1 Introduction

Tunneling effects are relevant in oscillating universe models obtained by recasting Friedmann dynamics in terms of the motion of the scale factor in a potential [1, 2]. Classical oscillations may then become unstable in quantum cosmology if at least one of the relevant potential barriers around the oscillation region are of finite height and width. Such instabilities have been studied in [3, 4] and, with an emphasis on tunneling, in [5–7].

Here, we demonstrate that not only the traditional tunneling probability familiar from stationary problems in standard quantum mechanics is of interest and computable, but also a more detailed picture of time-dependent tunneling dynamics. The methods we use, given by canonical effective descriptions of evolving quantum states based on the non-adiabatic dynamics of moments, have already proven useful in other fields, for instance by shedding light on the question of tunneling or traversal times [8–10] in atomic physics.

The quasiclassical method we apply here reformulates quantum dynamics of states as a coupled system of ordinary differential equations for expectation values of a basic set of operators together with higher moments. Such extended systems of equations could also be obtained classically if a distribution of like objects is considered instead of a single point particle [11, 12]. Quantum dynamics, however, not only introduces additional corrections in these equations for non-zero $\hbar$, it also gives the statistical degrees of freedom described by moments of a state a more fundamental role because they are then unavoidable. In general, the quantum state space is infinite-dimensional and hard to parameterize completely, but we will see that a single additional quantum parameter, identified with the size of quantum fluctuations and also used to parameterize higher moments in a suitable way, is sufficient to reveal interesting new features, in particular of the tunneling dynamics.

Even this restriced extension to one additional quantum degree of freedom and its canonically conjugate momentum reveals a quantum dynamics that is much more complicated than the regular classical one, and possibly chaotic. The classical dynamics of an isotropic universe as formulated in [1, 2] makes use of a 1-dimensional potential and is therefore guaranteed to be integrable.

Our extension by a single quantum parameter suffices to complicate the dynamics and possibly introduce chaotic features. We only provide circumstantial evidence for chaos in this paper and focus on a qualitative description of generic features of the extended dynamics. In particular, the additional parameter, compared with the classical formulation, implies that the universe, generically, enters different cycles of expansion and collapse with different initial

values of the quantum parameter. Since this parameter couples to the evolution of the scale factor, the latter reaches different maximum values in different cycles. Properties of cycles may therefore vary even if the matter ingredients and their parameters remain the same. In this way, a single model can give rise to a larger variety of universe cycles and more easily accomodate properties of a single observed universe.

2 Oscillating model

We start with the specific potential derived from an oscillating universe model introduced in [2]. The model is spatially isotropic, has positive spatial curvature, and an energy density given by

$$\rho(a) = \Lambda + \frac{\sigma}{a} + \rho_\phi \tag{2.1}$$

including a negative cosmological constant, $\Lambda < 0$, a matter density contribution σ/a with a positive constant $\sigma > 0$, as well as the energy density ρ_ϕ of a scalar field ϕ. The Friedmann equation therefore reads

$$\frac{\dot{a}^2}{a^2} + \frac{k}{a^2} = \frac{8\pi G}{3}\left(\Lambda + \frac{\sigma}{a} + \rho_\phi\right) . \tag{2.2}$$

As described in [7] for this model, the inclusion of a free, massless scalar field ϕ is useful because it implies two degrees of freedom, a and ϕ, that can evolve with respect to each other. Thus avoiding any reference to a time coordinate, which would not be subject to quantization, the scalar degree of freedom will help with the interpretation of dynamics in quantum cosmology following [13]. Note, however, that this relational evolution by itself does not solve the problem of time in quantum cosmology [14–16] because it requires a specific choice of time degree of freedom, ϕ, and is not guaranteed to provide quantum results independent of the choice of time [17–23].

The scalar being free of self-interactions and massless, its energy contribution is

$$\rho_\phi = \frac{p_\phi^2}{2a^6} \tag{2.3}$$

with the momentum p_ϕ of ϕ. Since there is no explicit ϕ-dependence, the scalar evolution equations imply that p_ϕ is a conserved quantity and that ϕ is monotonic with respect to any time coordinate as long as $p_\phi \neq 0$. Therefore, ϕ itself may be used as a global time coordinate to formulate quantum evolution of wave functions. Our methods will, however, be quasiclassical, as described in more detail below, and do not require the choice of a matter degree of freedom as time. Nevertheless, we keep the scalar energy density because it affects the dynamics of the scale factor through its appearance in the Friedmann equation. It may be considered a simple version of matter contributions not included in Λ and σ/a. Our specific results will only depend on the general feature that such energy contributions should be positive.

The curvature parameter k is positive by assumption and would equal $k = 1$ in the standard normalization of a if one assumes that all of isotropic space at any given time can be described as a complete 3-sphere. More generally, one may assume $0 < k < 1$ if the isotropic dynamics is interpreted as describing a collection of independent isotropic patches, approximating an inhomogeneous universe (as per [4], there are certain string effects that could also reduce the value of an effective k to be below one). According to the Belinskii-Khalatnikov-Lifshitz (BKL) scenario [24], the generic cosmological dynamics close to a spacelike singularity may indeed be approximated by a collection of independent homogeneous patches, although

JCAP05(2022)007

the generic dynamics would suggest a certain anisotropic geometry for each patch. As usual, the isotropic Friedmann equation serves as a simple first approximation to anisotropic but still homogeneous collapse or expansion. The value of k then determines the coordinate size of each patch as a fraction $k^{3/2}$ of the unit 3-sphere volume. Details of the BKL scenario show that, classically, homogeneous spatial patches close to a spacelike singularity are asymptotically small without a non-zero lower bound. The near-big bang behavior should therefore be described by small k. Since small k correspond to microscopic patches, their dynamics is usually more sensitive to various quantum effects than the dynamics of a single macroscopic space with $k = 1$ [25].

The patch model is particularly relevant for tunneling questions because it provides meaning to a tunneling probability, or to our description below in terms of expectation values and moments of a state. These statistical concepts require an ensemble of universe models, which in the patch picture can be individual constituents of the single universe that we are able to observe.

2.1 Potential

Given the sign choice of the cosmological constant, the Friedmann equation can be rewritten as the zero-energy condition

$$0 = \dot{a}^2 + \omega^2(a - \gamma/\omega)^2 + k - \gamma^2 - \frac{\tilde{p}^2}{a^4} = \dot{a}^2 + U_{\text{harmonic}}(a) - \frac{\tilde{p}^2}{a^4} \tag{2.4}$$

where

$$U_{\text{harmonic}}(a) = \omega^2(a - \gamma/\omega)^2 + k - \gamma^2 \tag{2.5}$$

is, up to constant shifts, a standard harmonic-oscillator potential with

$$\omega = \sqrt{-\frac{8\pi G\Lambda}{3}} \quad \text{and} \quad \gamma = \sqrt{-\frac{2\pi G\sigma^2}{3\Lambda}}\,. \tag{2.6}$$

The scalar density provides an anharmonic contribution determined by the constant

$$\tilde{p} = \sqrt{\frac{4\pi G}{3}} p_\phi\,. \tag{2.7}$$

The canonical formulation of the model does not look quite the same as the standard harmonic oscillator because the canonical momentum of a, according to general relativity, is not simply a constant times $\dot{a}$ but rather given by

$$p_a = -\frac{3}{4\pi G} a\dot{a}\,. \tag{2.8}$$

(Heuristically, as explained in more detail in [26], since the universe has no matter-independent mass that could be used to form a momentum from $\dot{a}$, an additional factor of a in combination with Newton's constant G is required.) Upon replacing $\dot{a}$ in (2.4) with p_a, the ω-term in the canonical potential of

$$0 = \frac{16}{9}\pi^2 G^2 p_a^2 + a^2 U_{\text{harmonic}}(a) - \tilde{p}^2 \tag{2.9}$$

is therefore quartic in a.

JCAP05(2022)007

The scale factor in a strict sense takes values in a semi-bounded range, given by positive numbers. Its canonical quantization therefore requires a suitable treatment of a phase space with a boundary, as undertaken for instance in [27–30] by applying methods from affine quantum gravity [31, 32]. Alternatively, one may first perform a canonical transformation from (a, p_a) to a canonical pair, (α, p_α), suitable for a logarithmic scale factor α. As in [7], we use the logarithmic scale factor

$$\alpha = \ln(\omega\gamma a)\,, \tag{2.10}$$

employing the two parameters (2.6) that characterize the harmonic potential (2.5). The definition (2.10) is turned into a canonical transformation if it is accompanied by

$$p_\alpha = a p_a = -\frac{3}{4\pi G} a^2 \dot{a}\,. \tag{2.11}$$

The canonical energy equation for (α, p_α) therefore reads

$$0 = \frac{16}{9}\pi^2 G^2 p_\alpha^2 + \frac{1}{\omega^4\gamma^4} e^{4\alpha} U_{\rm harmonic}(a(\alpha)) - \tilde{p}^2\,. \tag{2.12}$$

Defining

$$\beta = \frac{4\pi G}{3}\omega^2\gamma^2 \quad \text{and} \quad p = \frac{3}{4\pi G}\tilde{p}\,, \tag{2.13}$$

we finally obtain the basic dynamical equation

$$0 = p_\alpha^2 + U_p(\alpha) \tag{2.14}$$

with the potential

$$U_p(\alpha) = \frac{e^{4\alpha}}{\beta^2}\left(k - 2e^\alpha + \frac{e^{2\alpha}}{\gamma^2}\right) - p^2\,. \tag{2.15}$$

This potential is illustrated in figures 1 and 2 for different values of γ and k, respectively (the influence of β on the potential is easy to see because this parameter simply appears in a multiplier of the potential, except for the constant shift by $-p^2$). The dependence on both parameters is rather sensitive and determines the width and depth of the regions of classical oscillations. Moreover, choosing smaller k at fixed γ reduces the height of the barrier and can, for non-zero p, reduce the maximum to a value below zero, making it possible for the classical universe to collapse into a singularity ($\alpha \to -\infty$). The BKL-type fragmentation of space modeled by homogeneous patches close to a spacelike singularity, which requires smaller and smaller k as the universe collapses in order to maintain the homogeneous approximation, is therefore a new source of instability of oscillating universe models. Since we are mainly interested in analyzing the dynamics of quantum tunneling, assuming that it is relevant for the instability because the classical model would be stable, we will work with the value $k = 1$ in what follows.

Before we introduce quantum effects, we mention that evolution in proper time is generated by the constraint via Hamilton's equations. The relevant Hamilton function, as usual, is an energy expression, which is not the same as the standard kinetic energy plus an effective potential (2.15) used to visualize the motion in terms of barriers and allowed regions. The proper-time Hamiltonian differs from the right-hand side of (2.12) by multiplication with a suitable power of a or $\exp(\alpha)$, up to constants, because we have been multiplying the matter energy with several such factors in the process of performing transformations. Tracing back all these steps, proper-time evolution should be generated by the right-hand side of (2.12)

JCAP05(2022)007

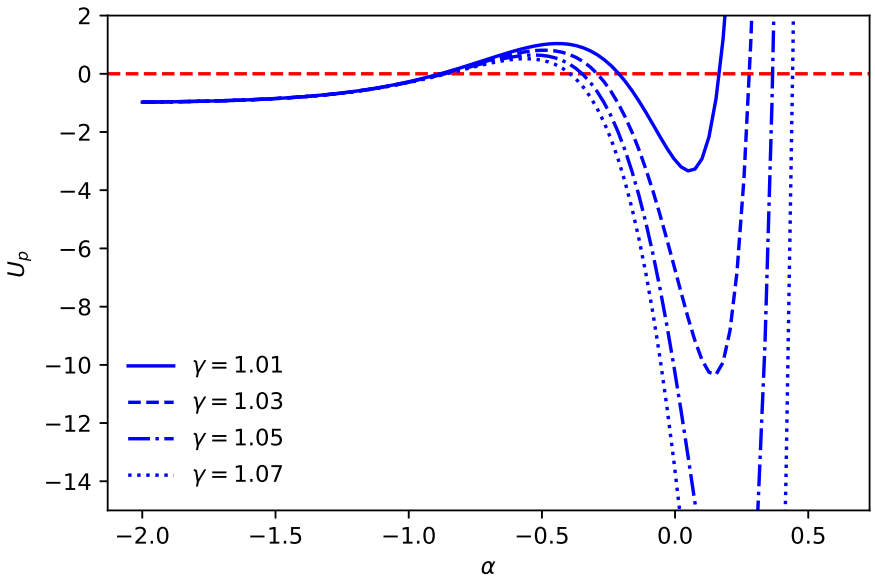

Figure 1. The potential (2.15) for different values of γ: $\gamma = 1.01$ (solid), $\gamma = 1.03$ (dashed), $\gamma = 1.05$ (dash-dotted) and $\gamma = 1.07$ (dotted). The dependence on γ is rather sensitive and determines the width and depth of confined regions with classical oscillations. The other parameters used in this plot are $k = 1$, $\beta = 0.1$ and $p = 1$.

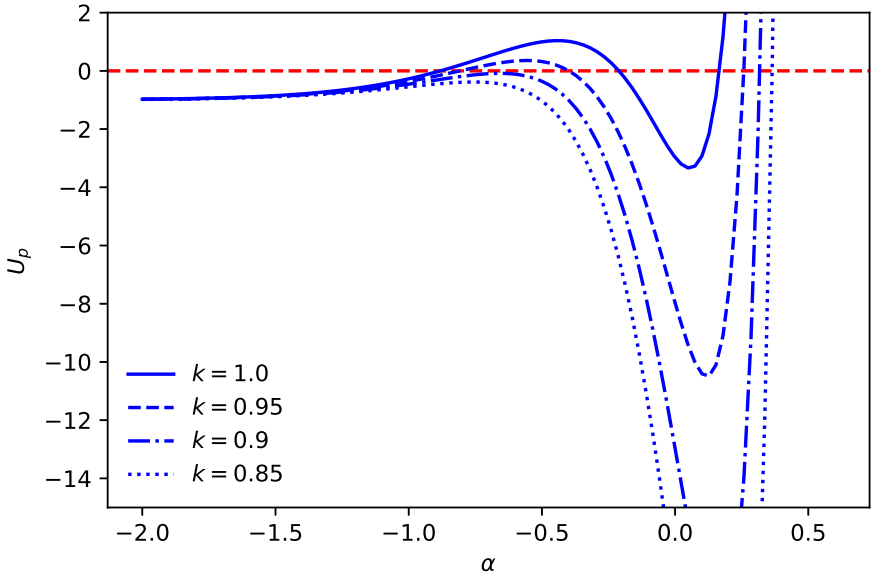

Figure 2. The potential (2.15) for different values of k: $k = 1.0$ (solid), $k = 0.95$ (dashed), $k = 0.9$ (dash-dotted) and $k = 0.85$ (dotted). The other parameters are $\gamma = 1.01$, $\beta = 0.1$ and $p = 1$.

times $\exp(-3\alpha)$. Up to constant factors, this multiple turns the p-term into the energy of a free, massless scalar field and therefore provides the correct generator of evolution. We may still use the potential landscape according to (2.15) to visualize the dynamics, but for quantitative estimates of time durations we should keep in mind that proper-time evolution is slowed down for larger α compared with what the potential would suggest. (We noticed

JCAP05(2022)007

that including the exponential factor of $\exp(-3\alpha)$ for proper-time dynamics complicates the numerical solution of differential equations because the factor changes quickly in some regions of the relevant phase space.)

2.2 Canonical effective methods

For a semiclassical description of tunneling dynamics, it is important to use non-adiabatic methods that allow one to go beyond stationary states. A suitable canonical formulation can be obtained by writing wave-function dynamics in terms of a dynamical system for expectation values of basic operators, such as $\hat{\alpha}$ and $\hat{p}_\alpha$, in a state coupled to fluctuations and higher moments, generically

$$\Delta(\alpha^a p_\alpha^b) = \langle(\hat{\alpha} - \langle\hat{\alpha}\rangle)^a(\hat{p}_\alpha - \langle\hat{p}_\alpha\rangle)^b\rangle_{\rm symm} \tag{2.16}$$

in completely symmetric, or Weyl, ordering. A phase-space structure is obtained for these variables by defining the Poisson bracket

$$\{\langle\hat{A}\rangle, \langle\hat{B}\rangle\} = \frac{\langle[\hat{A},\hat{B}]\rangle}{i\hbar} \tag{2.17}$$

and extending it to moments by using the Leibniz rule [33, 34].

While $\{\langle\alpha\rangle, \langle\hat{p}_\alpha\rangle\} = 1$ according to this definition, the Poisson bracket of moments is non-canonical. (For instance, $\{\Delta(\alpha^2), \Delta(p_\alpha^2)\} = 4\Delta(\alpha p_\alpha)$.) The transformation from the 3-dimensional space of second-order moments to new variables (s, p_s, U), defined by

$$\Delta(\alpha^2) = s^2 \tag{2.18}$$

$$\Delta(\alpha p_\alpha) = s p_s \tag{2.19}$$

$$\Delta(p_\alpha^2) = p_s^2 + \frac{U}{s^2}\,, \tag{2.20}$$

turns out to imply a canonical bracket $\{s, p_s\} = 1$ while $\{U, s\} = 0 = \{U, p_s\}$ (these canonical variables have been introduced several times independently for various studies of semiclassical dynamics [35–40]). The parameter U, which equals the uncertainty expression $\Delta(\alpha^2)\Delta(p_\alpha)^2 - \Delta(\alpha p_\alpha)^2$ as a consequence of the mapping (2.18)–(2.20), is therefore a Casimir variable of the Poisson manifold. That is, it has vanishing Poisson brackets with basic expectation values and all second-order moments and is conserved by any canonical dynamics of these variables. Heisenberg's uncertainty relation implies the lower bound $U \geq \hbar^2/4$.

Given a Hamilton operator $\hat{H}$, a canonical effective Hamiltonian can be derived by inserting the mapping (2.18)–(2.20) in the expectation value $\langle\hat{H}\rangle$. For us, the relevant expression is given by the constraint (2.14) with the non-polynomial potential (2.15). A Taylor expansion of the potential — formally in $\Delta\hat{\alpha} = \hat{\alpha} - \langle\hat{\alpha}\rangle$, after inserting $\langle\hat{\alpha}\rangle + \Delta\hat{\alpha}$ in the quantum operator $\langle U_p(\hat{\alpha})\rangle$ — implies the moment-corrected constraint

$$0 = \langle\hat{p}_\alpha\rangle^2 + \Delta(p_\alpha^2) + U_p(\langle\hat{\alpha}\rangle) + \sum_{n=2}^{\infty} \frac{1}{n!} \frac{{\rm d}^n U_p(\langle\hat{\alpha}\rangle)}{{\rm d}\langle\hat{\alpha}\rangle^n} \Delta(\alpha^n) \tag{2.21}$$

with an infinite series of higher moments. Including only moments of second order and using (2.18)–(2.20) as well as the simplified notation $\alpha = \langle\hat{\alpha}\rangle$ and $p_\alpha = \langle\hat{p}_\alpha\rangle$, we obtain the canonical expression

$$0 = p_\alpha^2 + p_s^2 + \frac{U}{s^2} + U_p(\alpha) + \frac{1}{2} U_p''(\alpha) s^2 \tag{2.22}$$

for our semiclassical constraint.

JCAP05(2022)007

Tunneling processes rely on higher-order moments because wave packets not only spread out, as described by the variance $\Delta(\alpha^2)$, but also split up into reflected and tunneled wave packets; see also [41]. An extension of the canonical mapping (2.18)–(2.20) to higher orders is challenging, not the least because the dimension of the Poisson manifold quickly increases when new moments are included as independent degrees of freedom. For explicit mappings to canonical variables for moments of third and fourth order, see [8, 9].

Instead of using a full mapping to higher orders, closure conditions have proven useful in studies of tunneling. Such conditions present an approximate description of higher-order moments in terms of lower-order parameters such as s, without including additional degrees of freedom for them. An example would be a Gaussian closure because for a Gaussian state, all moments are determined by second-order ones. A slightly different example that is algebraically simpler in effective potentials is the all-orders closure proposed in [10], where

$$\Delta(\alpha^n) = s^n \tag{2.23}$$

for even n while $\Delta(\alpha^n) = 0$ for odd n. With this closure, the whole series in (2.21) can be summed explicitly to obtain the simple constraint

$$0 = p_\alpha^2 + p_s^2 + \frac{U}{s^2} + \frac{1}{2}\left(U_p(\alpha+s) + U_p(\alpha-s)\right) . \tag{2.24}$$

A similar expression of effective potentials for certain classes of states has also been derived from Wigner functions [42].

The dynamics generated by the closure (2.24) is described by the same number of variables as the dynamics generated by the truncation (2.22). A closure condition makes additional assumptions about the relationships between higher-order moments and lower-order ones, while a truncation simply ignores higher-order moments. In general, the specific situation should determine whether a closure or a truncation is preferred. In tunneling examples, as in the present case, a truncation is usually harder to control because a potential barrier (given by a local maximum if the potential is smooth) implies a negative second derivative, making the last term in (2.22) unbounded from below. The all-orders potential (2.24), by contrast, is bounded from below provided the classical potential is bounded from below. It is therefore less likely (although not impossible) that effective trajectories derived from an all-orders Hamiltonian veer quickly toward larger values of s where the approximation would no longer be reliable.

We will use the all-orders closure in our analysis, illustrated in figure 3, but will also see that it is beneficial to include an additional quartic term in s to bring the fourth-order moment, $\Delta(\alpha^4)$, closer to its Gaussian value, $\Delta(\alpha^4) = 3s^4$ rather than s^4 (similar parameterizations of moments have been used in other cosmological analyses, such as [43, 44]). The constraint then reads

$$0 = p_\alpha^2 + p_s^2 + \frac{U}{s^2} + \frac{1}{2}\left(U_p(\alpha+s) + U_p(\alpha-s)\right) + \frac{1}{12}U_p''''(\alpha)s^4 . \tag{2.25}$$

(The last term equals $2U_p''''s^4/4!$, which increases the fourth-order term $U_p''''s^4/4!$ contained in the all-orders contribution to the Gaussian value of $3U_p''''s^4/4!$.) Additional amendments at higher moment orders may also be considered, but they will not play a large role in the first analysis presented here because the main new effects we will point out are realized at small values of s where polynomial contributions to the potential of higher degree in s are suppressed. We will, in fact, discard parts of solutions that reach larger values of s,

JCAP05(2022)007

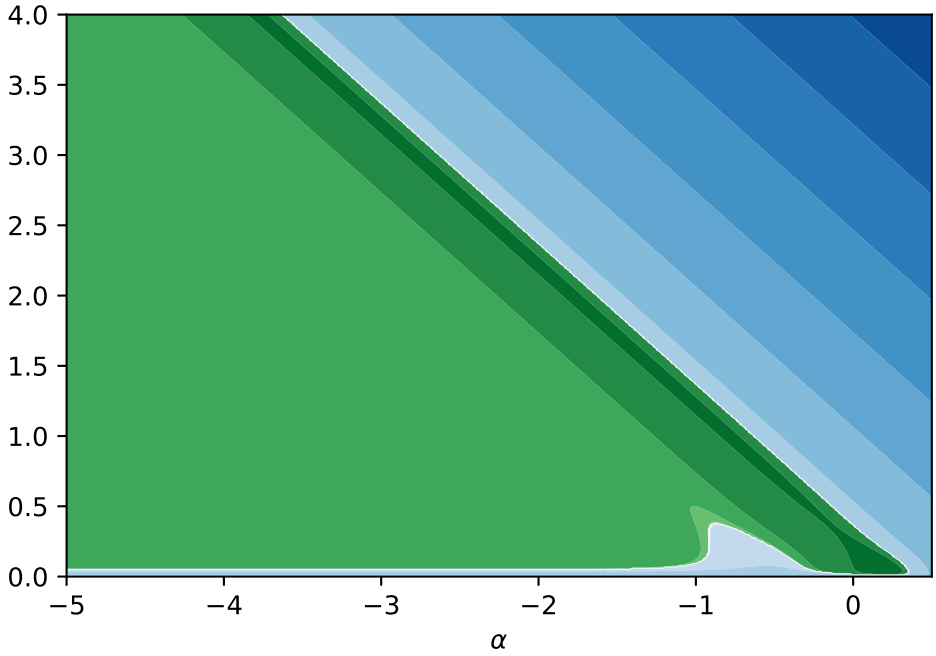

Figure 3. Logarithmic plot of the quantum potential in (2.24) for $\gamma = 1.05$, $\beta = 0.1$, $p = 1.0$ and $4U = 10^{-2}$. The classical barrier around $\alpha = -0.5$ is reduced in the s-direction while it moves to smaller α. Around $s = 0.5$ at $\alpha \approx -1$, the barrier height falls below zero, such that the left-most region connects with a channel of negative potential that ends at the classically confined region. Tunneling out of the classically confined region can therefore be described quasi-classically by motion in an extended phase-space, by-passing the classical barrier while maintaining energy conservation. The quantum variable s has to grow sufficiently large during tunneling in order to bypass the classical barrier, which physically corresponds to the increase of the variance of a state as it splits up into reflected and tunneled wave packets. The color scale is logarithmic with greens for negative values of the potential and blues for positive values.

considering them unreliable within the current approximation. Nevertheless, specific forms of closure conditions (or truncations) may have an effect on the resulting dynamics if the latter may be chaotic and therefore depend sensitively on small changes. This is indeed one of the properties indicated by our analysis. Further studies with different or more general closure conditions are therefore needed to understand the full dynamics. However, since the main purpose of the present paper is to show the possibility of chaos and related qualitative features, we are confident that these conclusions will not be removed when other closures are considered. It should also be kept in mind that different closures do not only constitute different approximations to the dynamics, but also describe physically distinct classes of states.

2.3 Approximations

A characteristic qualitative feature of the effective potential $\frac{1}{2}(U_p(\alpha + s) + U_p(\alpha - s))$ is an extension of the classical confined region to a channel that reaches smaller α for larger s; see figure 3: if the local minimum of the potential in the confined region is located at α_0, the extended potential at $(\alpha, s(\alpha))$ along the line $s(\alpha) \approx \alpha_0 - \alpha$ is much smaller than the classical potential $U_p(\alpha)$ because $U_p(\alpha + s(\alpha)) \approx U_p(\alpha_0)$ is much smaller than $U_p(\alpha)$ as well as $U_p(\alpha - s)$. The classical confined region is therefore extended into a channel along

JCAP05(2022)007

$s(\alpha) \approx \alpha_0 - \alpha$ in the (α, s)-plane. The additional quartic contribution in (2.25) preserves the channel and only modifies its width for small s (see figure 10 below).

Properties of the channel are important for tunneling dynamics. The channel tends to guide trajectories toward larger values of s. On one hand, this behavior seems qualitatively correct in a tunneling process during which wave packets are expected to split up. However, moving too far along the channel makes a trajectory unreliable or increases its sensitivity to different closure conditions. As we will discuss in more detail, we will therefore be interested in solutions that eventually leave the channel rather than getting stuck in it for a long time. A mathematical characterization of the channel, given in this subsection, will support such an analysis.

Characteristic channel features are given by the zero levels of the extended potential in the (α, s)-plane as well as the s-dependent location of the local maximum in the α-direction. The potential and its α-derivative are polynomials in $\exp(\alpha)$ of higher than quadratic order, such that exact expressions for the zero levels and local maxima would be hard to find, or lengthy. Fortunately, since the walls of the channel are rather steep for common parameter choices, the subtraction of p^2 does not significantly change the zero levels, and it does not change local extrema at all. For sufficiently large s, we can ignore the $1/s^2$-term. Moreover, around the barrier, whose properties are described by the local maxima as well as one of the zero levels at smaller α, the γ-term in the potential can be ignored because α is negative in this region. The right-most zero level is located at positive α, where the k-term in the potential can be ignored.

These approximations lead to simple equations for the desired quantities, given by

$$e^{\alpha_{\max}(s)} = \frac{2k}{5} \frac{\cosh(4s)}{\cosh(5s)} \tag{2.26}$$

for the local maxima in the α-direction,

$$e^{\alpha_{\text{left}}(s)} = \frac{k}{2} \frac{\cosh(4s)}{\cosh(5s)} \tag{2.27}$$

for the left zero level, and

$$e^{\alpha_{\text{right}}(s)} = 2\gamma^2 \frac{\cosh(4s)}{\cosh(5s)} \tag{2.28}$$

for the right zero level. For relatively large s, these equations can be simplified further by using $\cosh(x) \approx \frac{1}{2}e^x$ for $x \gg 1$. Thus, we arrive at

$$\alpha_{\max}(s) \approx \ln(2k/5) - s \quad , \quad \alpha_{\text{left}}(s) \approx \ln(k/2) - s \quad , \quad \alpha_{\text{right}}(s) \approx \ln(2\gamma^2) - s\,. \tag{2.29}$$

Figure 4 demonstrates the reliability of these approximations.

The classical local maximum, located at $\alpha_{\max}(0) = \ln(2k/5)$, has a height of

$$U_{\max} = \frac{k}{5\beta^2} \left(\frac{2k}{5}\right)^4 - p^2\,, \tag{2.30}$$

using the same approximation as in the derivation of $\alpha_{\max}(s)$. The value of the extended potential decreases along $\alpha_{\max}(s)$. In the limit of very large s, we can ignore contributions from $\exp(\alpha - s)$ in the extended potential while $\exp(\alpha + s)$, according to (2.29) becomes

JCAP05(2022)007

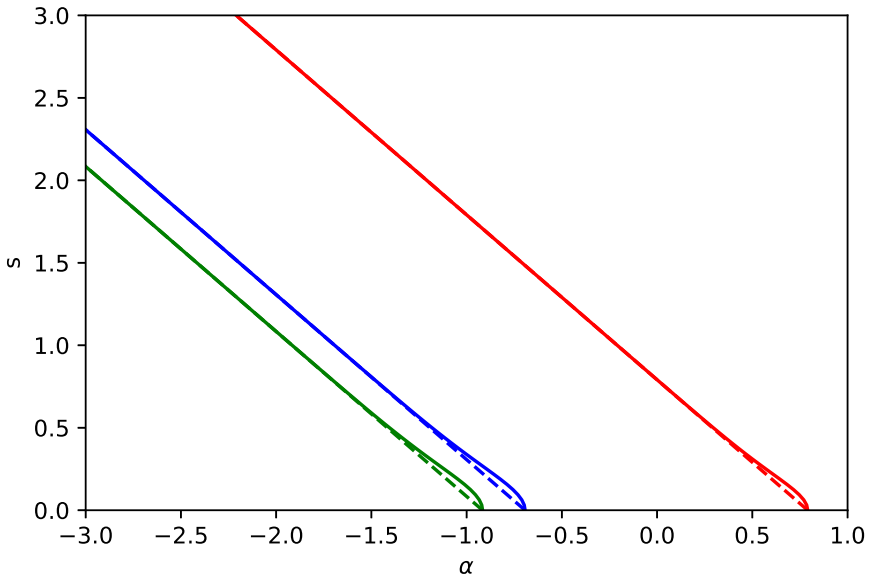

Figure 4. Characterization of the channel, given by the local maxima in the α-direction (green), the left side of the channel (blue) and its right side (red). Dashed lines show the approximations (2.29). The relevant parameters are $k = 1$ and $\gamma = 1.05$.

independent of s. With these approximations, we can see that the maxima in the α-direction approach a constant value which turns out to equal

$$\lim_{s\to\infty}\left(U_p(\alpha_{\max}(s), s) + p^2\right) = \frac{k}{10\beta^2}\left(\frac{2k}{5}\right)^4 = \frac{1}{2}\left(U_{\max} + p^2\right) . \tag{2.31}$$

For the barrier to disappear by quantum effects for the class of states described by our closure condition, we therefore need $p^2 > \frac{1}{2}(U_{\max} + p^2)$, or $p^2 > U_{\max}$. The full dependence of the local maxima in the α-direction is shown in figure 5.

2.4 Features of tunneling trajectories

We have numerically analyzed evolution in our versions of quantum potentials, using rather small values for γ in order to avoid steep potential walls on which reflections of an evolving trajectory are hard to resolve. The case of cosmological interest would rather be large values of γ that imply a large confined region which models long-term expansion of a universe. The small values of γ used here nevertheless allow us to infer interesting qualitative features of trajectories that are expected to hold also for large γ.

Quantum potentials such as (2.22), (2.24) or (2.25) show how tunneling dynamics can be realized in classical-type motion without violating energy conservation. For instance, the second derivative in (2.22) is negative around a local maximum, and therefore the quantum potential is lower than the classical barrier for non-zero s. In the present case, the averaging of U_p at $\alpha + s$ and $\alpha - s$ contained in (2.24) and (2.25) not only implies a similar lowering of the barrier, as shown in figure 6, but also extends the classically oscillating region into a channel that reaches to negative values of α for sufficiently large s; see figure 3.

A negative potential at zero energy does not necessarily imply that a trajectory can cross the barrier if there are more than one dimension. In one dimension, the momentum is non-zero under these conditions and the object keeps moving in the same direction, but in

JCAP05(2022)007

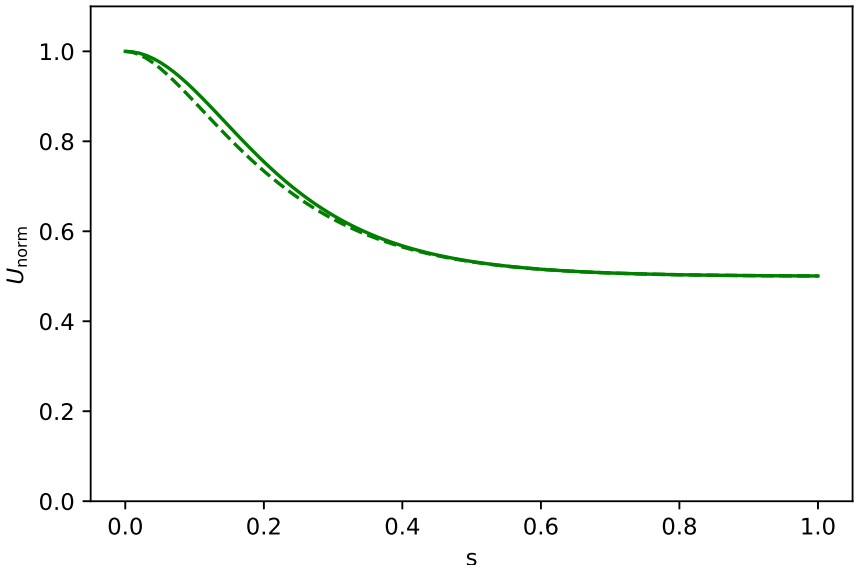

Figure 5. Behavior of the barrier height as a function of s, normalized to unit height of the classical barrier: $U_{\mathrm{norm}}(s) = (U_p(\alpha_{\mathrm{max}}(s), s) + p^2)/(U_{\mathrm{max}} + p^2)$. The dashed line is based on the simplified expression of $\alpha_{\mathrm{max}}(s)$ in (2.29).

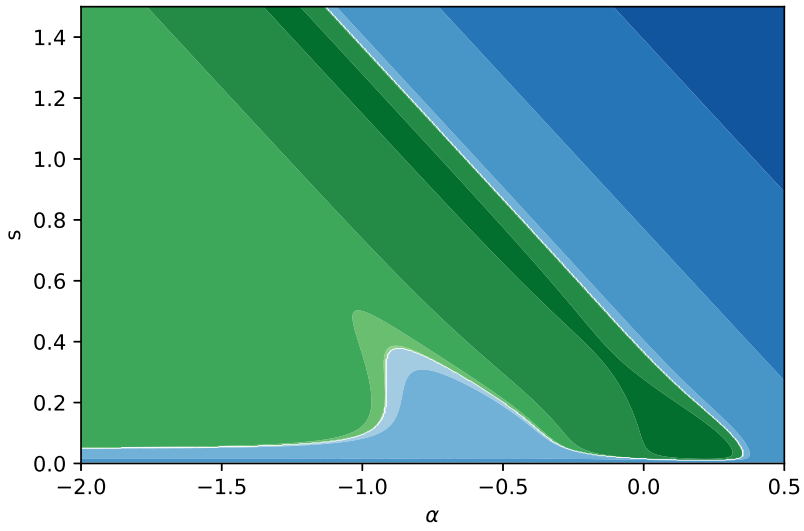

Figure 6. Larger range of the quantum potential with the same parameters and color scale as in figure 3.

two or more dimensions an object can get deflected and turn around while its momentum remains non-zero. Based on numerical simulations with random initial values that start around $\alpha = 0$ and small s, we have found that trajectories often get stuck in the channel and keep moving along it to larger and larger s. At such large s, the channel is very straight such that a trajectory, once it reaches this region, follows a periodic pattern between deflections at the channel walls without moving out. While the channel guides the trajectory toward smaller α, very far to the left of the classical barrier, we do not consider these solutions to

JCAP05(2022)007

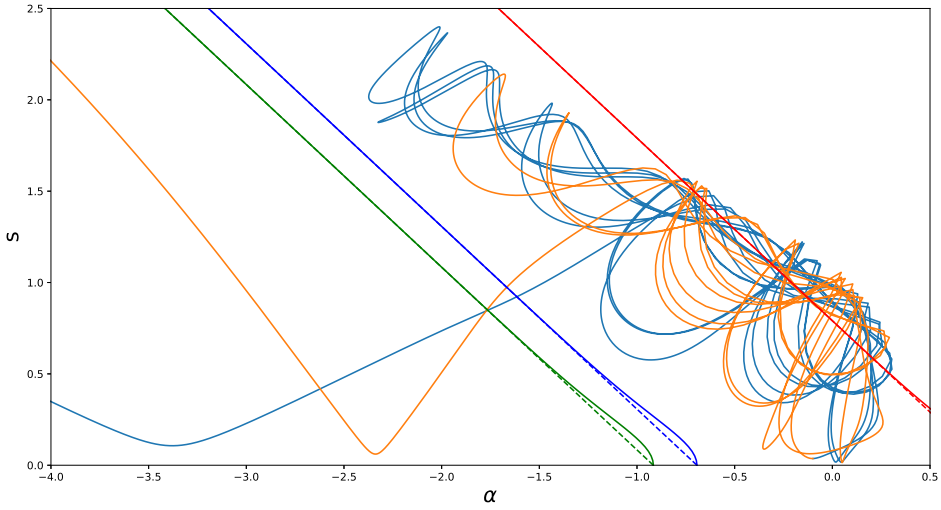

Figure 7. Tunneling trajectory in the amended all-orders potential (2.25). The diagonal lines indicate characteristic features of the non-amended wall as in figure 4. The additional quartic contribution in the amended potential allows the trajectory to penetrate the right wall of the channel at small s. Blue and orange parts of the trajectory indicate times before and after a random initial condition, respectively.

be good examples of tunneling because our quasiclassical approximation and the moment closure become unreliable at large s.

Deviations from the all-orders closure, as implied by contributions from higher moments different from (2.23), make the channel irregular, such that a trajectory bounces off the channel walls at different angles each time, making it more likely to exit the channel eventually. At very large s, several higher-order moments are relevant in an amended closure. It is then hard to derive generic information without prior knowledge of the tunneling state and its moments. Fortunately, as shown by figures 7 and 8, the fourth-order amendment of the potential in (2.25) makes it possible to find trajectories that enter and exit the channel at rather small s. The additional fourth-order contribution to the potential, shown in figures 10 and 11, keeps the trajectory closer to the end of the channel at smaller s, where it has several opportunities to probe the channel wall under different impact directions and eventually crosses the barrier.

As can be seen in figure 7, s reaches large values also to the left of the classical barrier, where this variable keeps increasing after a single reflection at small s, caused by the U/s^2 contribution to the potential. This increase to large values is expected because the classical potential is nearly constant in this region. The trajectory therefore behaves like the quantum fluctuation $s = \Delta\alpha$ of a free particle, which increases before and after its minimum value, changing linearly for asymptotically large times.

It is noteworthy that the minima of s in the nearly free region are located close to the classical barrier before and after tunneling in and out of the trapped region. This behavior is expected if one imagines a wave function approaching a barrier, such that it gets more narrow as some of its front part starts getting reflected back toward the center. Similarly, a wave packet that tunnels out of the trapped region may narrow down briefly when only a small contribution is left in the trapped region. Based on the extended potential as a function of α and s, the minima of the free region are generically located near the barrier because the

JCAP05(2022)007

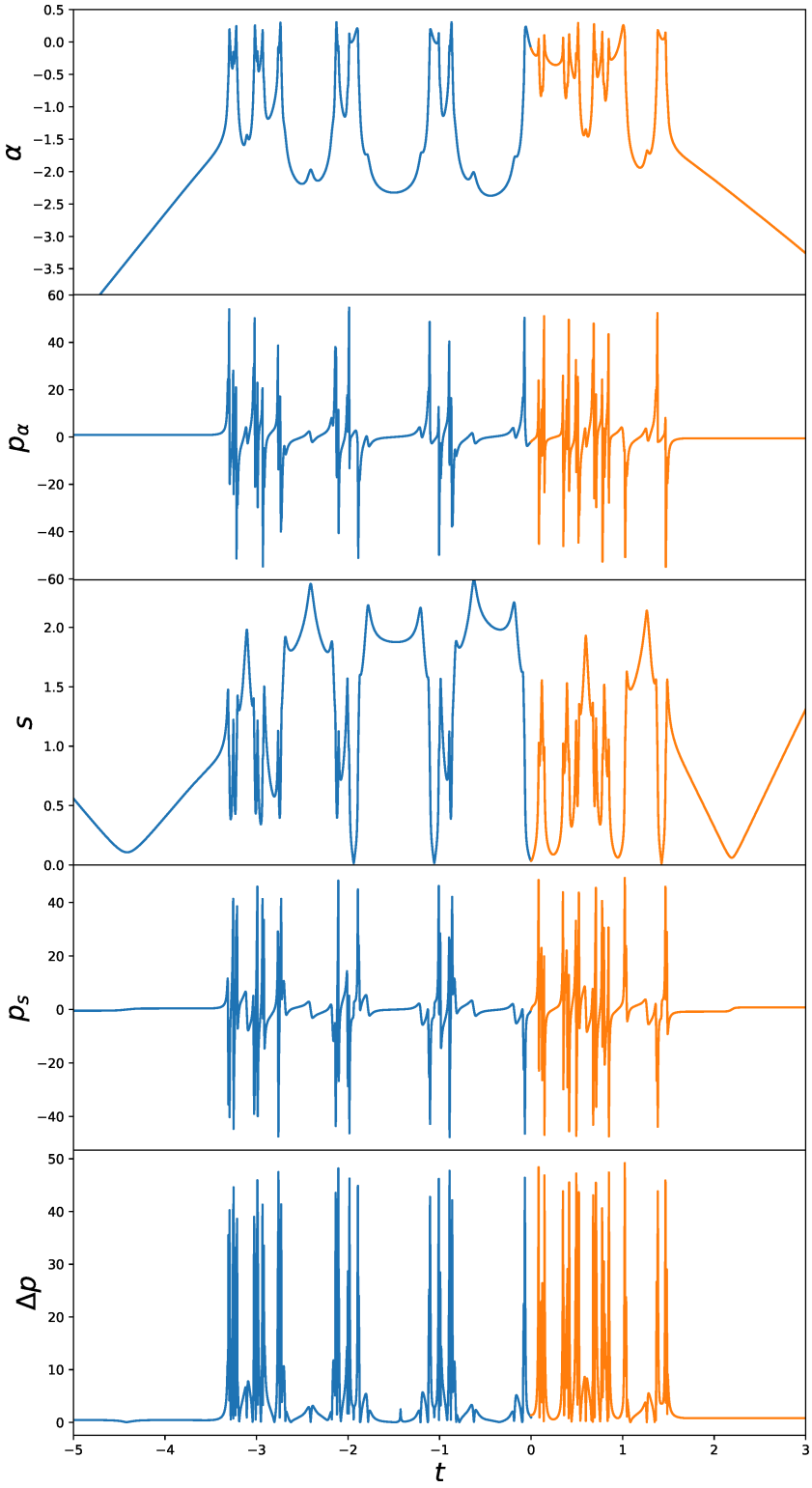

Figure 8. Details of the tunneling trajectory shown in figure 7. A random initial condition has been set where the blue and orange curves meet.

JCAP05(2022)007

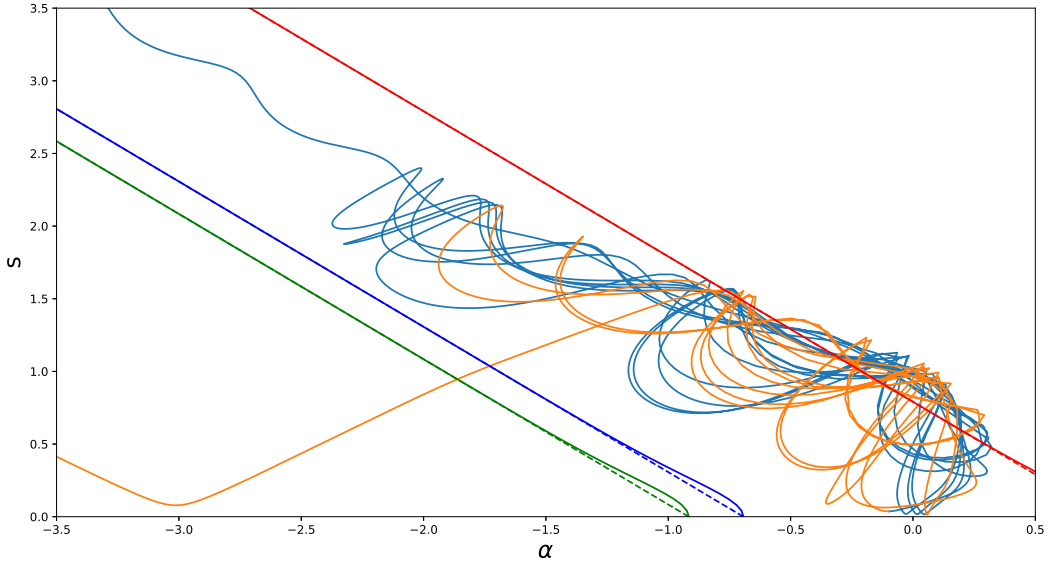

Figure 9. Tunneling trajectory in the amended all-orders potential (2.25). All parameters are the same as in figure 7, except that the initial value of α has been changed from -0.09938693911314142 to -0.09938693911314141, a difference only in the last relevant decimal place. The final outcome of this tiny change is very large because the trajectory now gets stuck in the channel.

trajectory has to approach the channel wall, located between the blue and green lines in the figure, at close to a right angle. Under this condition it is able to move through and escape, rather than being deflected back into the channel. The direction of the channel implies that escaping trajectories are aimed toward smaller s, toward the U/s^2-potential where they reach their local minima.

Our quasiclassical trajectories therefore provide a meaningful and geometrical description of the beginning and the end of a tunneling process. The trapped part of the trajectory is harder to interpret, but it is clear that it is much more complicated than the classical solution in this region, which at constant energy would oscillate with a regular period and amplitude. The combined evolution of α and s, by contrast, has neither a regular period nor a fixed amplitude, even though the quantum energy, given by our effective Hamiltonian, is conserved. The complicated nature of quantum dynamics in the trapped region is also highlighted by a high sensitivity to initial values, as seen by comparing figure 7 with figure 9.

The sensitivity to initial values is reminiscent of chaos, although we have not performed a detailed analysis to demonstrate this feature. The classical system is clearly non-chaotic (being 1-dimensional), but quantum dynamics may nevertheless develop chaotic features as known for instance from Bohmian treatments [45]. Another indication that the extended dynamics here may be chaotic can be seen in the shape of the trapped region in the amended all-orders potential, shown in figures 10 and 11. As shown by the contours, the trapped region is confined by walls that are partially concave, which may support chaotic billiard motion as in other cosmological models, such as anisotropic ones [46].

We note that our effective potentials could also be used to describe the classical dynamics of an ensemble of patches of space whose volume distribution has a certain variance s^2. The main place where our dynamics depends on a non-zero value of $\hbar$ is in the term U/s^2 of the effective potentials, where U is a constant bounded from below by $\hbar^2/4$. The s^{-2}-behavior

JCAP05(2022)007

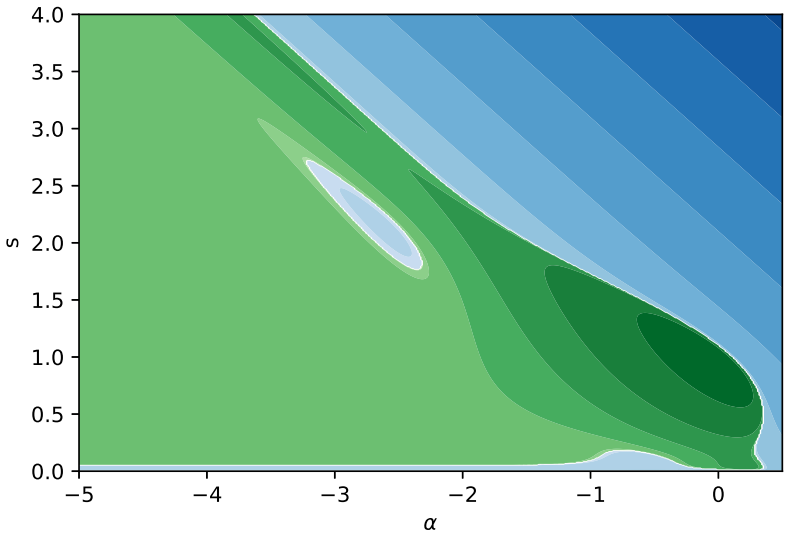

Figure 10. The amended potential (2.25) with the same parameters as in figure 3.

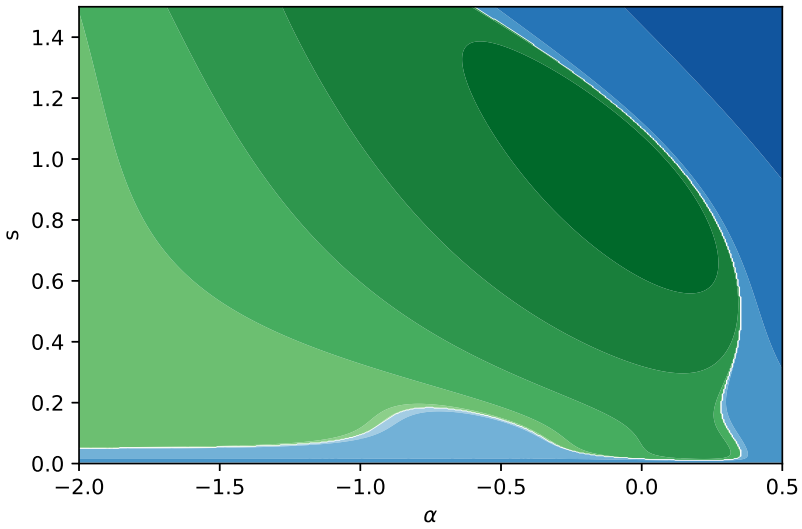

Figure 11. Closer view of the end of the channel from figure 10.

of this term implies a potential barrier at small s that enforces the uncertainty relation. Classically, U can be as small as we like, removing the potential barrier. Differences between quantum dynamics and classical ensemble dynamics should therefore be most pronounced at small s. Both cases are likely subject to chaos because they share relevant features of an extension from the α-line to an (α, s)-plane. However, as our sample trajectories show, specific instances of the dynamics encounter small s multiple times. Reflections on the s^{-2}-potential in the quantum dynamics would classically be replaced by sharp reflections at $s = 0$ or (depending on the treatment) transition through $s = 0$ to negative values while the variance s^2 stays non-negative. While both cases are likely to be chaotic, this feature also implies that classical and quantum dynamics would differ significantly from each other after small s are encountered by a trajectory.

JCAP05(2022)007

3 Conclusions

Our analysis of extended quantum potentials has suggested a strategy to find and study quasiclassical tunneling solutions for an oscillating universe model. We derived quantum corrections to the classical potential based on an assumption about the moment closure of states. A closure condition is unlikely to describe all relevant states, but it can reveal some properties of dynamical tunneling, provided solutions stay in regions in which the closure condition can be considered a good approximation. For instance, a precise closure at higher orders of moments should not be required if the fluctuation variable, s, remains sufficiently small.

While a full quantum treatment would imply that any state initially supported in the oscillating region will eventually tunnel and approach the singularity at $\alpha \to -\infty$, perhaps after separating into several wave packets that had tunneled at different times, our quasiclassical description implies tunneling only under certain conditions on the initial values of a trajectory. In particular, although the value of s should not become too big for our approximations to be valid, it has to grow sufficiently large close to the classical barrier for the local maximum in the α-direction (one of the channel walls) to have dropped below zero. This condition cannot be fulfilled for all parameter values but requires, in partiular, that the parameter p that determines the asymptotic potential at $\alpha \to -\infty$ is sufficiently large. If p is too small, we would not see any quasiclassical tunneling solutions in our model even though quantum tunneliung in a full treatment would certainly occur. Quasiclassical models of the form considered here, therefore, cannot provide a complete description of tunneling. But solutions that stay within the allowed ranges of parameters may still provide interesting dynamical information that would be harder to find using traditional methods.

Our main result is the observation that oscillations in the trapped region, seen over many cycles, are much less regular in the quantum case than they appear classically. Our numerical simulations were restricted to small γ, or rather narrow trapped regions, because the steep potential walls implied by larger values of this parameter make it hard to achieve reliable numerics. Qualitatively, larger γ imply longer cycles in the trapped region, which may give the appearance of more regular behavior because the new quantum variable, s, does not change as abruptly during a single cycle as it does after multiple reflections off the potential walls. Nevertheless, the succession of several cycles should also be less regular than in the classical case if γ is large because each cycle generically starts with different values of s and p_s, which affect the evolution of α through quantum back-reaction. A single model may therefore probe a large number of cosmological cycles with different maximal expansion, even if matter parameters remain the same.

A quasiclassical model may also be crucial in developing a scenario that couples the isotropic background to perturbative anisotropies or inhomogeneity. Such a combination would be harder to analyze at the full quantum level where a combined wave function for background and inhomogeneity would have to be evaluated. It may be easier, by comparison, to couple a quasiclassical background model to a standard description of perturbative inhomogeneity and analyze how quantum effects could affect the evolution of inhomogeneous modes through a tunneling process.

Acknowledgments

We thank Ning Ni for discussions. This work was supported in part by NSF grant PHY-1912168.

JCAP05(2022)007

References

[1] M.P. Dabrowski, *Oscillating Friedman cosmology*, *Annals Phys.* **248** (1996) 199 [gr-qc/9503017] [INSPIRE].

[2] P.W. Graham, B. Horn, S. Kachru, S. Rajendran and G. Torroba, *A simple harmonic universe*, *JHEP* **02** (2014) 029 [arXiv:1109.0282] [INSPIRE].

[3] A.T. Mithani and A. Vilenkin, *Instability of an emergent universe*, *JCAP* **05** (2014) 006 [arXiv:1403.0818] [INSPIRE].

[4] P.W. Graham, B. Horn, S. Rajendran and G. Torroba, *Exploring eternal stability with the simple harmonic universe*, *JHEP* **08** (2014) 163 [arXiv:1405.0282] [INSPIRE].

[5] M.P. Dabrowski and A.L. Larsen, *Quantum tunneling effect in oscillating Friedmann cosmology*, *Phys. Rev. D* **52** (1995) 3424 [gr-qc/9504025] [INSPIRE].

[6] A.T. Mithani and A. Vilenkin, *Collapse of simple harmonic universe*, *JCAP* **01** (2012) 028 [arXiv:1110.4096] [INSPIRE].

[7] A.T. Mithani and A. Vilenkin, *Tunneling decay rate in quantum cosmology*, *Phys. Rev. D* **91** (2015) 123511 [arXiv:1503.00400] [INSPIRE].

[8] B. Baytas, M. Bojowald and S. Crowe, *Faithful realizations of semiclassical truncations*, *Annals Phys.* **420** (2020) 168247 [arXiv:1810.12127] [INSPIRE].

[9] B. Baytaş, M. Bojowald and S. Crowe, *Effective potentials from semiclassical truncations*, *Phys. Rev. A* **99** (2019) 042114 [arXiv:1811.00505] [INSPIRE].

[10] B. Baytaş, M. Bojowald and S. Crowe, *Canonical tunneling time in ionization experiments*, *Phys. Rev. A* **98** (2018) 063417 [arXiv:1810.12804] [INSPIRE].

[11] D. Brizuela, *Statistical moments for classical and quantum dynamics: formalism and generalized uncertainty relations*, *Phys. Rev. D* **90** (2014) 085027 [arXiv:1410.5776] [INSPIRE].

[12] D. Brizuela, *Classical and quantum behavior of the harmonic and the quartic oscillators*, *Phys. Rev. D* **90** (2014) 125018 [arXiv:1411.1522] [INSPIRE].

[13] W.F. Blyth and C.J. Isham, *Quantization of a Friedmann universe filled with a scalar field*, *Phys. Rev. D* **11** (1975) 768 [INSPIRE].

[14] K.V. Kuchař, *Time and interpretations of quantum gravity*, in *Proceedings of the 4th Canadian Conference on General Relativity and Relativistic Astrophysics*, G. Kunstatter, D.E. Vincent and J.G. Williams, eds., World Scientific, Singapore (1992).

[15] C.J. Isham, *Canonical quantum gravity and the problem of time*, in *Integrable systems, quantum groups, and quantum field theory*, pp. 157–287, Kluwer, Dordrecht (1993).

[16] E. Anderson, *The problem of time in quantum gravity*, arXiv:1009.2157 [INSPIRE].

[17] M. Bojowald and T. Halnon, *Time in quantum cosmology*, *Phys. Rev. D* **98** (2018) 066001 [arXiv:1612.00353] [INSPIRE].

[18] P. Małkiewicz, *Multiple choices of time in quantum cosmology*, *Class. Quant. Grav.* **32** (2015) 135004 [arXiv:1407.3457] [INSPIRE].

[19] P. Malkiewicz, *Clocks and dynamics in quantum models of gravity*, *Class. Quant. Grav.* **34** (2017) 145012 [arXiv:1601.04857] [INSPIRE].

[20] P. Małkiewicz, P. Peter and S.D.P. Vitenti, *Quantum empty Bianchi I spacetime with internal time*, *Phys. Rev. D* **101** (2020) 046012 [arXiv:1911.09892] [INSPIRE].

[21] P.A. Höhn, *Switching internal times and a new perspective on the 'wave function of the universe'*, *Universe* **5** (2019) 116 [arXiv:1811.00611] [INSPIRE].

[22] S. Gielen and L. Menéndez-Pidal, *Singularity resolution depends on the clock*, *Class. Quant. Grav.* **37** (2020) 205018 [arXiv:2005.05357] [INSPIRE].

[23] S. Gielen and L. Menéndez-Pidal, *Unitarity, clock dependence and quantum recollapse in quantum cosmology*, *Class. Quant. Grav.* **39** (2022) 075011 [arXiv:2109.02660] [INSPIRE].

JCAP05(2022)007

[24] V.a. Belinsky, I.m. Khalatnikov and E.m. Lifshitz, *A general solution of the Einstein equations with a time singularity*, *Adv. Phys.* **31** (1982) 639 [INSPIRE].

[25] M. Bojowald, *The BKL scenario, infrared renormalization, and quantum cosmology*, *JCAP* **01** (2019) 026 [arXiv:1810.00238] [INSPIRE].

[26] M. Bojowald, *Foundations of quantum cosmology*, IOP Publishing, London, U.K. (2020).

[27] H. Bergeron, E. Czuchry, J.-P. Gazeau, P. Małkiewicz and W. Piechocki, *Smooth quantum dynamics of the mixmaster universe*, *Phys. Rev. D* **92** (2015) 061302 [arXiv:1501.02174] [INSPIRE].

[28] H. Bergeron, E. Czuchry, J.-P. Gazeau, P. Małkiewicz and W. Piechocki, *Singularity avoidance in a quantum model of the Mixmaster universe*, *Phys. Rev. D* **92** (2015) 124018 [arXiv:1501.07871] [INSPIRE].

[29] H. Bergeron, E. Czuchry, J.-P. Gazeau and P. Małkiewicz, *Spectral properties of the quantum Mixmaster universe*, *Phys. Rev. D* **96** (2017) 043521 [arXiv:1703.08462] [INSPIRE].

[30] H. Bergeron, E. Czuchry, J.-P. Gazeau and P. Małkiewicz, *Quantum mixmaster as a model of the primordial universe*, *Universe* **6** (2019) 7 [arXiv:1911.02127] [INSPIRE].

[31] J.R. Klauder, *Affine quantum gravity*, *Int. J. Mod. Phys. D* **12** (2003) 1769 [gr-qc/0305067] [INSPIRE].

[32] J.R. Klauder, *Overview of affine quantum gravity*, *Int. J. Geom. Meth. Mod. Phys.* **3** (2006) 81 [gr-qc/0507113] [INSPIRE].

[33] M. Bojowald and A. Skirzewski, *Effective equations of motion for quantum systems*, *Rev. Math. Phys.* **18** (2006) 713 [math-ph/0511043] [INSPIRE].

[34] M. Bojowald and A. Skirzewski, *Quantum gravity and higher curvature actions*, *eConf* **C 0602061** (2006) 03 [hep-th/0606232] [INSPIRE].

[35] R. Jackiw and A. Kerman, *Time dependent variational principle and the effective action*, *Phys. Lett. A* **71** (1979) 158 [INSPIRE].

[36] F. Arickx, J. Broeckhove, W. Coene and P. van Leuven, *Gaussian wave-packet dynamics*, *Int. J. Quant. Chem.* **20** (1986) 471.

[37] R.A. Jalabert and H.M. Pastawski, *Environment-independent decoherence rate in classically chaotic systems*, *Phys. Rev. Lett.* **86** (2001) 2490.

[38] O. Prezhdo, *Quantized hamiltonian dynamics*, *Theor. Chem. Acc.* **116** (2006) 206.

[39] T. Vachaspati and G. Zahariade, *Classical-quantum correspondence and backreaction*, *Phys. Rev. D* **98** (2018) 065002 [arXiv:1806.05196] [INSPIRE].

[40] M. Mukhopadhyay and T. Vachaspati, *Rolling classical scalar field in a linear potential coupled to a quantum field*, *Phys. Rev. D* **100** (2019) 096018 [arXiv:1907.03762] [INSPIRE].

[41] L. Aragon-Muñoz, G. Chacon-Acosta and H. Hernandez-Hernandez, *Effective quantum tunneling from a semiclassical momentous approach*, *Int. J. Mod. Phys. B* **34** (2020) 2050271 [arXiv:2004.00118] [INSPIRE].

[42] E.J. Heller, *Wigner phase space method: analysis for semiclassical applications*, *J. Chem. Phys.* **65** (1976) 1289.

[43] M. Bojowald, S. Brahma, S. Crowe, D. Ding and J. McCracken, *Quantum Higgs inflation*, *Phys. Lett. B* **816** (2021) 136193 [arXiv:2011.02355] [INSPIRE].

[44] M. Bojowald, S. Brahma, S. Crowe, D. Ding and J. McCracken, *Multi-field inflation from single-field models*, *JCAP* **08** (2021) 047 [arXiv:2011.02843] [INSPIRE].

[45] G. Contopoulos and A.C. Tzemos, *Chaos in bohmian quantum mechanics: a short review*, *Regul. Chaot. Dyn.* **25** (2020) 476 [arXiv:2009.05867].

[46] T. Damour, M. Henneaux and H. Nicolai, *Cosmological billiards*, *Class. Quant. Grav.* **20** (2003) R145 [hep-th/0212256] [INSPIRE].

JCAP05(2022)007